sustainability

MDPI

Article

Jet Flame Risk Analysis for Safe Response to Hydrogen Vehicle Accidents

Byoungjik Park [1], Yangkyun Kim [1], Jin Ouk Park [1] and Ohk Kun Lim [2,*]

[1] Hydrogen-Infrastructure Research Cluster, Korea Institute of Civil Engineering and Building Technology, Goyang-si 18544, Gyeonggi-do, Republic of Korea; templer83@kict.re.kr (B.P.); yangkyunkim@kict.re.kr (Y.K.); jopark@kict.re.kr (J.O.P.)

[2] Department of Police Science, Dong-A University, Busan-si 49236, Republic of Korea

* Correspondence: oklim@dau.ac.kr; Tel.: +82-51-200-8673

Abstract: With an increase in the use of eco-friendly vehicles such as hybrid, electric, and hydrogen vehicles in response to the global climate crisis, accidents related to these vehicles have also increased. Numerical analysis was performed to optimize the safety of first responders responding to hydrogen vehicle accidents wherein hydrogen jet flames occur. The influence range of the jet flame generated through a 1.8-mm-diameter nozzle was analyzed based on five discharge angles (90, 75, 60, 45, and 30°) between the road surface and the downward vertical. As the discharge angle decreases toward the road surface, the risk area that could cause damage moves from the center of the vehicle to the rear; at a discharge angle of 90°, the range above 9.5 kW/m^2 was 1.59 m and 4.09 m to the front and rear of the vehicle, respectively. However, at a discharge angle of 30°, it was not generated at the front but was 10.39 m to the rear. In response to a hydrogen vehicle accident, first responders should perform rescue activities approaching from a diagonal direction to the vehicle front to minimize injury risk. This study can be used in future hydrogen vehicle design to develop the response strategy of the first responders.

Keywords: fuel-cell electric vehicle (FCEV); hydrogen jet flame; thermally activated pressure relief device (TPRD); first responder; incident response

Citation: Park, B.; Kim, Y.; Park, J.O.; Lim, O.K. Jet Flame Risk Analysis for Safe Response to Hydrogen Vehicle Accidents. *Sustainability* **2023**, *15*, 9884. https://doi.org/10.3390/su15139884

Academic Editors: Chao Xu, Ming Gao, Fuqiang Wang, Zhonghao Rao and Weihua Cai

Received: 23 April 2023
Revised: 12 June 2023
Accepted: 19 June 2023
Published: 21 June 2023

1. Introduction

The climate crisis is fueled by greenhouse gas emissions from various sources, including transportation, industrial processes, and power generation. In the United States, fossil fuels such as gasoline and diesel account for more than 90% of the fuel used in automobiles, ships, and trains. Greenhouse gases emitted from these transportation modes account for the largest share of total emissions at 27% [1]. In recent years, the use of vehicles with low carbon dioxide emissions, such as hybrid, electric, and hydrogen vehicles, requiring active infrastructure construction has increased. As of 2021, 729 hydrogen refueling stations have been installed globally, with 169 in Japan, 147 in China, and 114 in Korea, reflecting the transition to a hydrogen economy in Asian countries. Meanwhile, 54,437 hydrogen vehicles have been registered worldwide, of which 19,404 are in Republic of Korea and 12,358 in the United States, accounting for more than 60% of the total. Notably, passenger cars account for more than 82% of all hydrogen vehicles [2].

The proportion of eco-friendly vehicles registered in Republic of Korea has risen sharply from 0.7% in 2014 to 6.2% in December 2022, and of those, registrations of hydrogen vehicles have more than doubled every year [3]. Currently, no accidents involving hydrogen vehicles have been reported, but accidents involving electric vehicles (EVs) have been steadily increasing. The first EV accident occurred in 2017 in Republic of Korea, when 25,108 EVs were registered. As of April 2023, 31,805 hydrogen vehicles have been registered, indicating a potentially higher risk of accidents compared to that of EVs. Li et al. surveyed first responders in the United Kingdom on their awareness of safe response strategies to

hydrogen vehicle accidents [4]. Although 60% were aware of invisible hydrogen jet flames, they did not know that these flames are caused by gas discharge through the thermally activated pressure relief device (TPRD) installed on hydrogen storage tanks to prevent catastrophic tank rupture. Conversely, more than 70% responded that they were familiar with high-voltage circuits or electric cutoffs in electric vehicles. While the responders were aware of gas leaks or no-cut zones in hydrogen vehicles, they were unfamiliar with specific accident response procedures, and none have experienced an accident involving hydrogen vehicles. Since 2017, the number of studies related to hydrogen safety has been increasing; however, limited research has been conducted on effective incident response [5]. Therefore, new standard operating procedures and related resources must be prepared [6,7].

To date, no accidents involving hydrogen passenger vehicles have occurred in South Korea. However, in December 2021, the tire of a tube trailer vehicle transporting compressed hydrogen caught fire, activating the TPRD attached to the hydrogen storage container, resulting in an approximately 20 m-high vertical jet flame. Catastrophic tank rupture was avoided when the TPRD was activated, and the situation was resolved when a first responder extinguished the fire after the release of hydrogen. Generally, the pressure discharge of the TPRD is directed upwards in tube trailers carrying compressed hydrogen, and downwards toward the road surface in passenger cars. Emergency response guides for commercially available hydrogen vehicles specify that hydrogen gas should be discharged to the ground in case of an emergency [8,9]. These guides, which are provided by automobile manufacturers, specify risk factors such as immobilization and no-cut zones, but they do not suggest specific accident response plans for first responders.

Much research is being conducted on ensuring the safety of hydrogen facilities and equipment, such as hydrogen tanks and hydrogen refueling stations [10–12]. Hussein et al. investigated temperature variations in the release direction of a jet flame in a parking area and found that it was difficult for passengers to escape when the jet flame was released vertically [13]. Accidents that can occur in hydrogen passenger vehicles include leaks, jet flames, and explosions, but the one most likely to cause damage is a sudden burst of flame from the activation of the TPRD. Therefore, this study aims to analyze the risk range of the jet flame generated by the TPRD in the event of a hydrogen vehicle accident. These results could provide drivers and first responders with information to more safely respond to hydrogen vehicle accidents.

2. Analysis Models

2.1. Hydrogen Vehicle Model

Hydrogen vehicles are in production in South Korea and Japan, and new models have recently been launched in Germany and the United States. Model A, a hydrogen vehicle with a high market share, has a total hydrogen storage capacity of 156.6 L, comprising three 52.2 L Type IV containers installed under the vehicle, as shown in Figure 1. Approximately 6.3 kg of hydrogen can be charged into these tanks [14], which are arranged sequentially on the underside of the vehicle, between the luggage compartment and the rear seat. The distance between hydrogen tanks No. 1 and 2 is 675 mm, and the distance between No. 2 and 3 is 420 mm. Each hydrogen storage container is equipped with a TPRD, which activates at approximately 110 °C, as shown in Figure 1b, with the discharge direction pointing vertically downwards to the road surface [8]. In this study, Model A was used to analyze the risks of jet flames during accident response.

2.2. Hydrogen Leak Modeling

During a leak in a high-pressure hydrogen tank, a critical flow state is observed wherein the hydrogen gas passes through a Mach disk, creating a complex shock wave that slows the hydrogen gas to subsonic speeds. In order to reduce the computational complexity of choked flow analysis, a pseudo-diameter approach is used [15], which is based on mass conservation. This approach has been applied in previous studies analyzing high-pressure leaks or jet flames of various hydrocarbon and hydrogen gases [16–18].

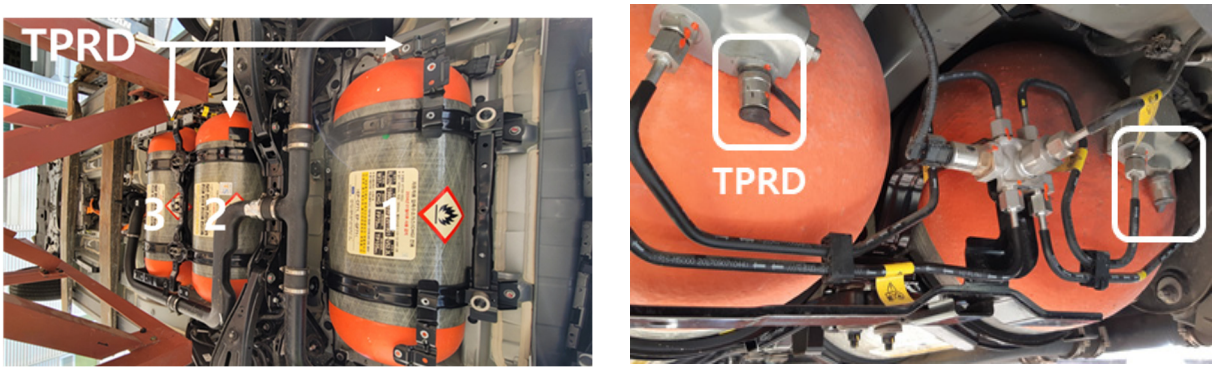

(**a**) (**b**)

Figure 1. Thermally activated pressure relief device (TPRD) and its venting position. (**a**) The underside of the fuel-cell electric vehicle (FCEV), and (**b**) TPRD installed on the hydrogen tank.

Figure 2 diagrams the release of supercritical gas from the tank. The pseudo-diameter (d_{ps}) was considered to be equal to the mass flow rate at ambient temperature and pressure with a uniform velocity. Three points are considered: the inside of the tank as an infinite reservoir (State 0), the tank orifice (State 1), and a point after the expansion, which is equal to ambient conditions (State 2).

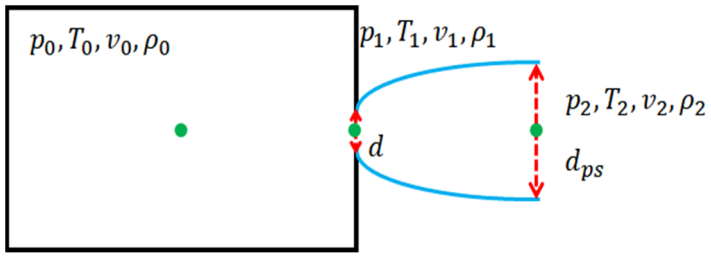

Figure 2. Diagrammatic representation of supercritical gas release.

Based on mass conservation, the relationship between States 1 and 2 can be derived as follows:

$$\frac{A_2}{A_1} = \frac{{d_{ps}}^2}{d^2} = \frac{C_d \rho_1 V_1}{\rho_2 V_2} \tag{1}$$

where A_1 is the area of the orifice, A_2 is the circular area calculated from the pseudo-diameter, C_d is the discharge coefficient, and ρ_1, ρ_2 and V_1, V_2 are the density and velocity of each state, respectively.

The tank wall is assumed to be adiabatic, viscous dissipation is ignored, and the released gas is considered to be an ideal gas. The flow from State 0 to State 1 is isentropic, and the density of the gas at State 1 can be derived as follows:

$$\rho_1 = \frac{P_0 \left(\frac{2}{k+1}\right)^{\frac{k}{k-1}} MW_{H_2}}{R_{H_2} T_0} \tag{2}$$

where k is the ratio of the heat capacity (k = 1.41), MW_{H_2} denotes the molar mass of the leaking gas, and R_{H_2} is the gas constant of hydrogen. From Equations (1) and (2), the following equations can be obtained:

$$V_1 = \sqrt{\frac{k R_{H_2} T_0 \frac{2}{k+1}}{MW_{H_2}}} \tag{3}$$

$$V_2 = \sqrt{\frac{kR_{H_2}T_2}{MW_{H_2}}} \tag{4}$$

$$\rho_2 = \frac{P_2 MW_{H_2}}{R_{H_2}T_2} \tag{5}$$

where T_0 and T_2 are the temperatures of each state, and P_2 is the ambient pressure.

By substituting the above equations and rearranging them, Equation (6) for the pseudo-diameter can be derived.

$${d_{ps}}^2 = C_d \frac{P_0}{P_2} \left(\frac{2}{k+1}\right)^{\frac{k+1}{2(k-1)}} \sqrt{\frac{T_2}{T_0}} d^2 \tag{6}$$

In this study, ANSYS Fluent 2021 R2, a commercial computational fluid dynamics (CFD) software based on the finite volume method (FVM), was used for CFD analysis. To simulate the hydrogen jet flame, the following mass, momentum, and energy conservation equations were used.

$$\frac{\partial \rho}{\partial t} + \nabla \cdot \left(\rho \vec{v}\right) = 0 \tag{7}$$

$$\frac{\partial}{\partial t}\left(\rho \vec{v}\right) + \nabla \cdot \left(\rho \vec{v} \vec{v}\right) = -p + \nabla \cdot \left(\bar{\bar{\tau}}\right) + \rho \vec{g} + \vec{F} \tag{8}$$

$$\frac{\partial}{\partial t}(\rho E) + \nabla \cdot \left(\rho \vec{v}\left(h + \frac{v^2}{2}\right)\right) = \nabla \left(k_{eff} \nabla T - \sum_j h_j \vec{J_j} + \bar{\bar{\tau}}_{eff} \cdot \vec{v}\right) \tag{9}$$

Papanikolau et al. compared several turbulence models using pseudo-diameter approaches and experimental data [19]. The shear stress transport (SST) k–ω turbulence model shows a smaller difference from the experimental data than the standard k–ε or baseline (BSL) k–ω model. In this study, the SST k–ω turbulence model was used to simulate the turbulence, the species transport equation to consider species reactions, and the discrete ordinates (DO) model was used for radiative heat transfer. In order to simulate the hydrogen combustion reaction, four chemical species were considered: H_2, O_2, H_2O, and N_2. Eddy dissipation was applied to the combustion model, which assumes that the hydrogen reaction rate is very high and dependent on turbulent mixing. The DO model was used to calculate the radiant heat flux caused by hydrogen combustion. The polar and azimuthal angles were set at 5°, and the pixels were set at 3 for analysis accuracy.

A hydrogen risk assessment model (HyRAM) was used to estimate the hydrogen leak rate of the TPRD nozzle over time, as shown in Figure 3. The detailed calculation conditions are presented in Table 1, and the exposure flow rate was calculated using Equation (10):

$$\frac{du}{dt} = \frac{\dot{m}(h-u)+q}{m} \tag{10}$$

where u and h denote the energy and enthalpy per unit mass of hydrogen gas, respectively, q denotes the heat transfer into the hydrogen storage container, and m denotes the mass of hydrogen gas stored in the container. In order to analyze changes in the jet flame with respect to time, a flow rate that decreases with time was applied as a boundary condition of the analysis based on the conditions in Table 1, as shown in Figure 3.

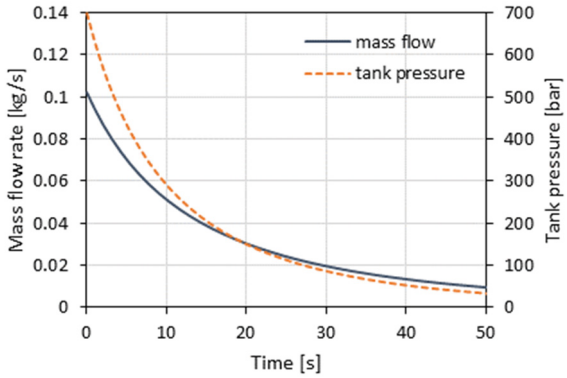

Figure 3. Mass flow rate and pressure change of the hydrogen tank.

Table 1. Hydrogen tank model parameters.

Volume (L)	Pressure (MPa)	Nozzle Size (mm)	Flow Rate (kg/s)	Length (mm)	Diameter (mm)
52.2	70	1.8	0.102	870	363

A coupled technique was used for pressure–velocity coupling in the pressure-based solver. First-order implicit transient analysis was applied, with no initial flow at the calculation area. The hydrogen gas flow was set to zero, and the oxygen and nitrogen volume fractions were equal to atmospheric conditions. The time step size was set to 0.01 s, and the analysis was conducted for 10 s.

Figure 4 shows the hydrogen vehicle and the grid used for jet flame analysis. In order to analyze the effects of the jet flame, a numerical analysis domain was set up as a rectangular parallelepiped spanning 10 m vertically from the floor of the vehicle, and 20 and 30 m from the TPRD toward the front and sides, and rear, respectively. The risks of altering the TPRD leakage angle were evaluated by considering five cases for the angle between the horizontal and the leak port of Tank 1 (90, 75, 60, 45, and 30°), as shown in Figure 4c.

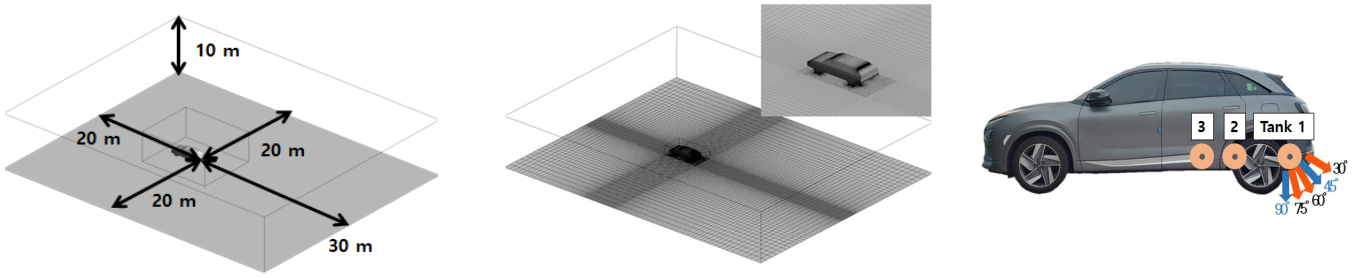

(**a**) (**b**) (**c**)

Figure 4. Schematic diagrams of the hydrogen vehicle modeling. (**a**) Calculation area, (**b**) calculation grid, and (**c**) TPRD discharge angle definition.

For computational efficiency and convergence, a dense grid was created around the vehicle and at the TPRD nozzle; the maximum and average skewness of the grid were 0.84 and 0.16, respectively, for computational convergence. In addition, about 2.1 million grids were created for each analysis condition using the sweep method on the vehicle periphery.

2.3. Validation

Before analyzing the hydrogen jet flame emitted from the TPRD of the vehicle, the CFD analysis methodology was validated by performing a numerical analysis under the same conditions as a previous physical experiment involving a jet flame against a concrete

wall [20]. As shown in Figure 5 the concrete wall was 1.8 m long and 0.25 m thick. The jet flame nozzle was installed 2 m from the wall. In this experiment, the injection nozzle of the jet flame was 1.8 mm, whereas, in the numerical analysis, the jet has a similar pseudo-diameter using the hydrogen leak modeling technique in Section 2.2. As in the experiment, a transient decrease of the flow rate from 53 to 50 g/s over 10 s was applied in the analysis. Apart from the boundary conditions, the calculation settings for the CFD analysis were the same as those presented in Section 2.2. In order to compare the numerical analysis and experimental results, the transient heat flux was measured at the eight monitoring points in Figure 5a. The monitoring points were selected at 1 m intervals in the longitudinal direction at 2 m from the center of the nozzle, similar to the experiment.

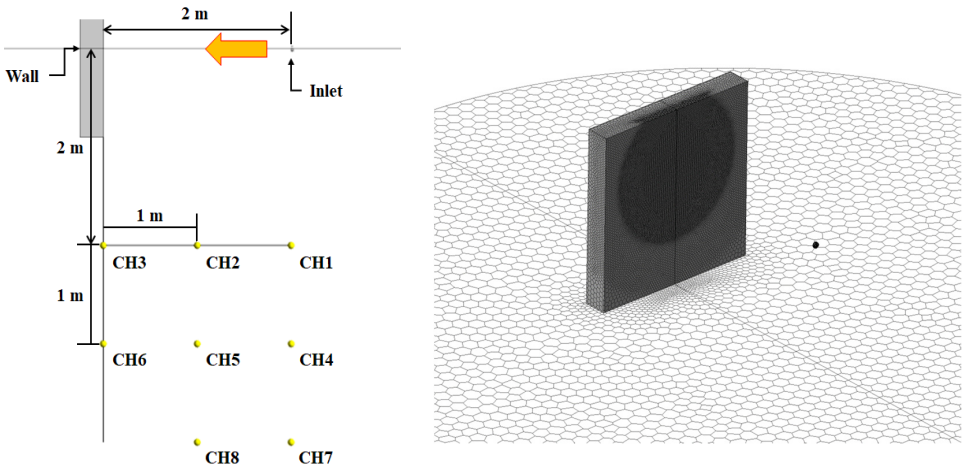

Figure 5. Schematic diagram and calculation grid for the CFD validation. (**a**) Calculation schematic and (**b**) calculation grid.

The temperature distribution at the central section of the leak after 10 s is shown in Figure 6a. A similar trend between the temperature distribution was observed through the thermal imaging camera in the experimental literature and the CFD analysis results. Figure 6b shows the radiant heat flux distribution at various time points during the analysis and the experiment. Complex fluctuations in the heat flux were observed at the initial time in the experiment, whereas no rapid change was observed in the CFD analysis. This can be attributed to the use of a pseudo-diameter for the discharge in the CFD analysis, while leakage occurs above the critical pressure during the experiment. As the experiment time elapsed, the radiant heat flux at each monitoring location was approximately 2–4 kW/m^2, depending on the distance from the jet flame. The heat flux results of the CFD analysis were in the range of 2–3 kW/m^2, which is consistent with the experimental results.

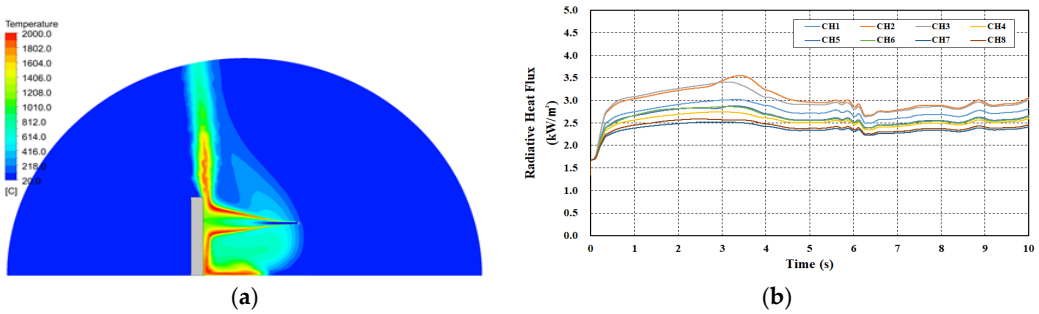

Figure 6. Results of the validation experiment. (**a**) Temperature contour—central view and (**b**) radiation heat flux with time.

3. Results and Discussion

3.1. Jet Flame Impact Range over Time

Figure 7 shows the heat flux distribution around the vehicle generated by the jet flame when hydrogen gas is released through a TPRD nozzle directed vertically toward the floor. Areas with heat fluxes exceeding 9.5 and 37.5 kW/m^2 are shown in green and red, respectively. Exposure to heat fluxes greater than 9.5 kW/m^2 for more than 20 s can cause second-degree burns on the human body. At a heat flux of 37.5 kW/m^2, serious damage can occur to both the human body and the mechanical equipment [21,22]. The distances from the vehicle where second-degree burns could occur were 1.59, 4.09, 4.48, and 3.91 m from the front, rear, left, and right sides of the vehicle, respectively. The jet flame generated by the rapidly discharging hydrogen gas passes through the lower part of the vehicle after hitting the floor, forming a high heat flux area around the vehicle, which could cause serious injuries to passengers exiting the vehicle. As shown in Figure 7b, a heat flux greater than 37.5 kW/m^2 encompassing the entire lower surface of the vehicle was generated up to about 3 m from the rear.

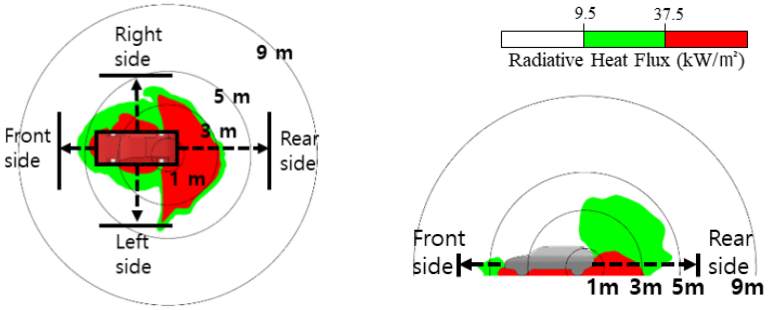

Figure 7. Radiative heat flux profiles around the vehicle with a 90° TPRD angle. (**a**) Plane view and (**b**) side view.

When the hydrogen compressed to 700 bar flows out of the storage container through the 1.8-mm-diameter nozzle, the flow rate and pressure in the container decrease exponentially, as presented in Figure 3. After approximately 10 s, the leakage flow rate is reduced to half its initial rate. Figure 8 shows the maximum range at which a heat flux greater than 9.5 kW/m^2 is generated around the vehicle by the jet flame, taking into account the transient decrease in the flow rate as the hydrogen is expelled. The burn risk area was observed to decrease over time across all sides of the vehicle. For example, it decreases from 4.09 to 2.53 m at the rear of the vehicle, and from 4.48 to 3.41 m at the left side of the vehicle. The burn risk area is largest at the onset of the jet flame and gradually decreases over time in a hydrogen vehicle accident.

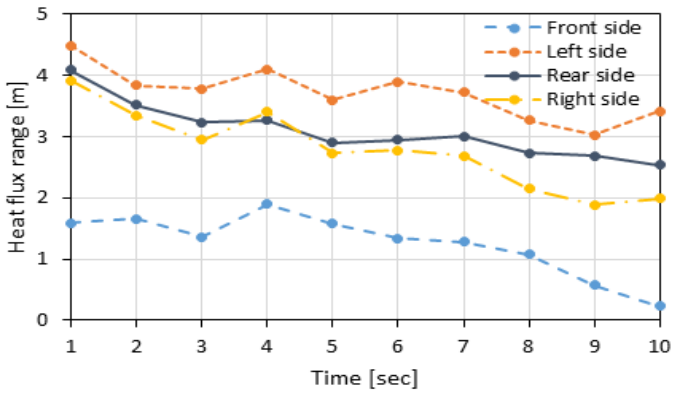

Figure 8. Maximum range of 9.5 kW/m^2 heat flux around the vehicle with a 90° TPRD discharge angle.

3.2. Analysis of Flame Range According to TPRD Angle

The hydrogen vehicle used in this study has three storage containers of equal capacity installed around the rear wheel axis of the vehicle. Assuming that the jet flame emanates from the rearmost container, as shown in Figure 4c, the heat flux range was analyzed by decreasing the jet angle to 30° from the horizontal. The analysis was conducted only for discharge angles greater than 30° because the exhaust gas would hit the bumper of the vehicle at smaller angles. As the angle of the TPRD decreases, the heat flux area moves from the center of the vehicle towards the rear, as illustrated in Figure 9. At a discharge angle of 60°, the risk area encompasses a 5 m radius centered on the hydrogen tank, whereas, at 45° or less, the risk area extends toward the rear of the vehicle but decreases in the sideways directions. Generally, TPRD outlets point vertically upwards in tube trailers or large trucks and downwards in passenger vehicles, with no regulation on the exact angle. As the angle of the outlet approaches 90°, the risk area encompasses the entire vehicle, thereby increasing the risk of injury to the occupants and first responders during a rescue. Conversely, as the discharge angle decreases, the risk area increases toward the rear of the vehicle, thereby increasing the possibility of secondary damage to nearby cars and buildings.

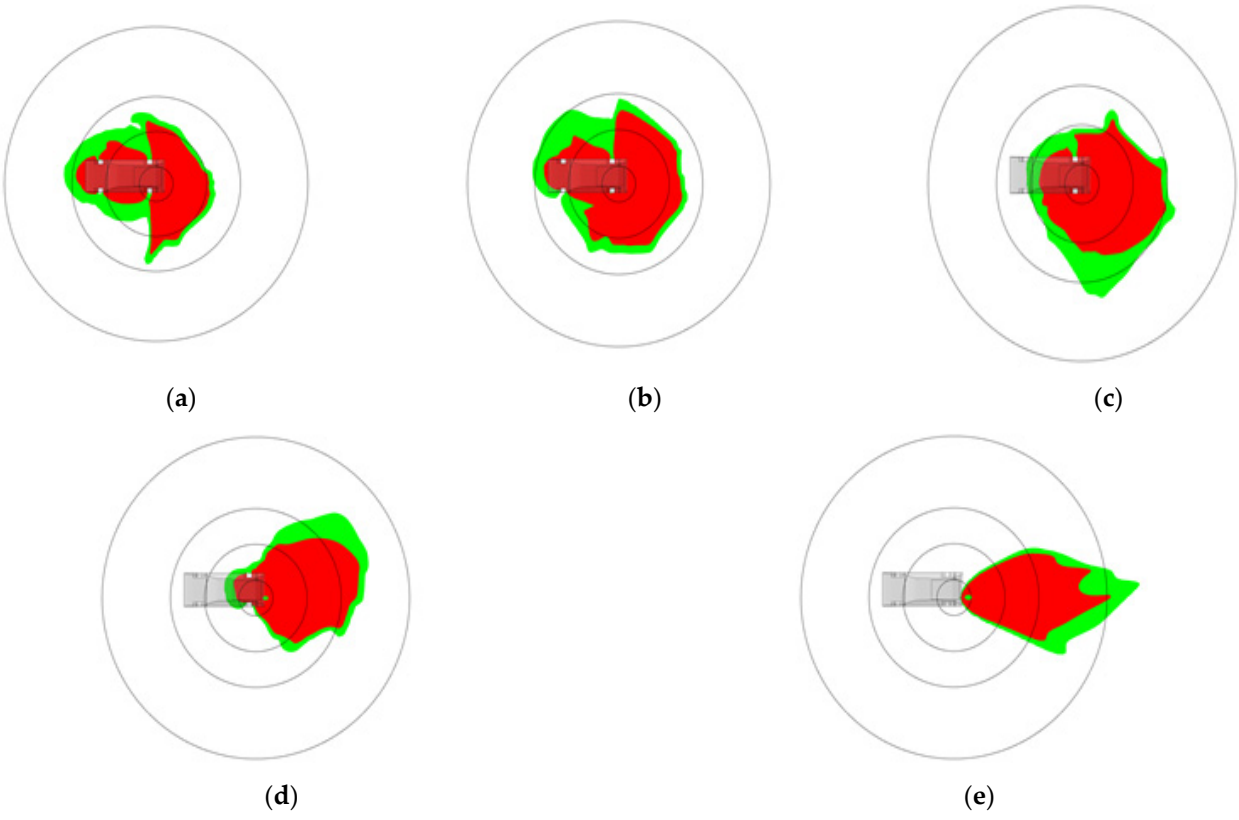

Figure 9. Heat flux profile around the vehicle at different TPRD discharge angles. (**a**) 90°, (**b**) 75°, (**c**) 60°, (**d**) 45°, and (**e**) 30°.

Figure 10 shows the maximum range of the heat flux formed around the vehicle according to the TPRD discharge angle. As the discharge angle decreases, the heat flux decreases on the front, left, and right of the car but increases in the rearward direction. Meanwhile, at discharge angles below 60°, harm-causing heat fluxes are not generated at the front of the vehicle but increasingly spread towards the rear of the vehicle. The left side of the vehicle is generally more affected by heat fluxes, as the TPRD on the hydrogen storage container is located on this side. The total length of the passenger car is approximately 4.5 m. At a discharge angle of less than 45°, a heat flux of 37.5 kW/m^2 can extend over 5.5 m towards the rear of the vehicle, potentially causing sequential damage such as tire

fires and adjacent TPRD operation. Meanwhile, at discharge angles less than 60°, an area of 9.5 kW/m^2 heat flux forms at a distance of 5 m on the left side and 3 m on the right side of the vehicle. However, the impact on the front seat of the passenger car is reduced, as illustrated in Figure 9c–e.

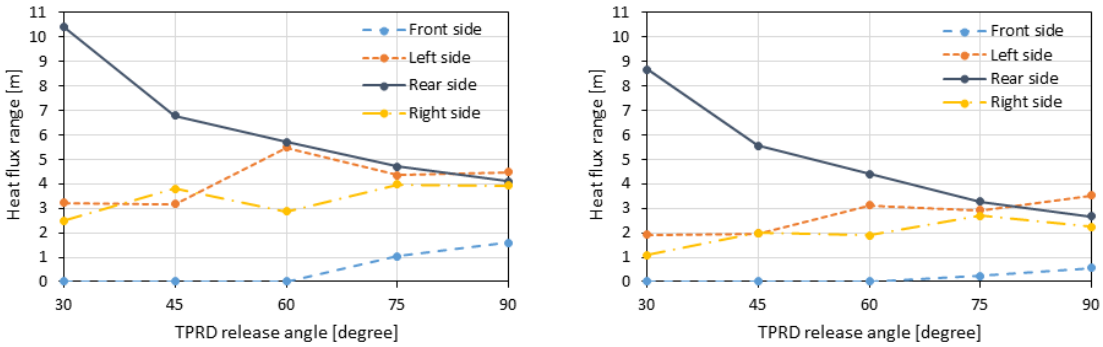

Figure 10. Maximum heat flux range depending on TPRD release angles. (**a**) 9.5 kW/m^2 range and (**b**) 37.5 kW/m^2 range.

The mean height measurements of males and females born in South Korea in 1996 are 1.7 m and 1.6 m, respectively [23], with eye levels typically being 0.1 m lower. While protective clothing can temporarily block radiative heat, the face remains exposed. The heat flux at 1.5 m (typical eye level) is illustrated in Figure 11 for each discharge angle. At a 90° discharge angle, heat fluxes exceeding 9.5 kW/m^2 were generated up to 5 m around the vehicle, which can cause second-degree burns. Notably, this range gradually shifts rearwards as the discharge angle decreases. In particular, an area with a heat flux of 37.5 kW/m^2 or more forms at discharge angles between 75° and 45° at the rear of the vehicle. When the jet flame is released between 90° and 75°, an area with a heat flux exceeding 9.5 kW/m^2 can form around the vehicle at a height of up to 1.5 m.

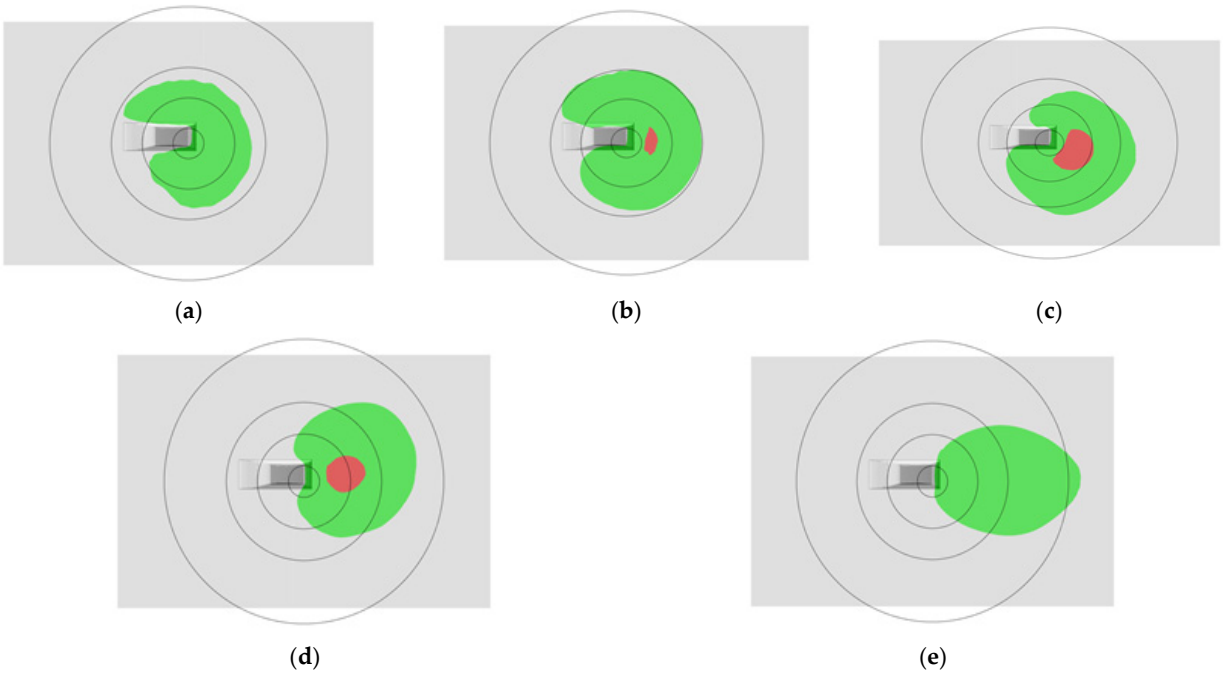

Figure 11. Heat flux profile around the vehicle at 1.5 m and different TPRD discharge angles. (**a**) 90°, (**b**) 75°, (**c**) 60°, (**d**) 45°, and (**e**) 30°.

3.3. Effects on Nearby Hydrogen Storage Container

Normally, when a fire occurs in a hydrogen vehicle, the TPRD is activated, and the internal hydrogen gas is expelled safely, preventing an explosion. We analyzed the probability of an adjacent hydrogen storage explosion when the TPRD of the hydrogen tank is activated, creating a jet flame. Blanc-Vannet et al. pressurized H_2, N_2, and He to 467 and 700 bar in 19 and 36 L Type IV tanks, and analyzed the temperatures through bonfire experiments [24]. When a heat flux of approximately 90 kW/m^2 was applied to the tank, it exploded between 160 and 311 s. Meanwhile, when the 36 L Type IV tank was pressurized to 700 bar, it exploded after 240 s, with an applied energy of 21.6 MJ/m^2. When the jet flame was generated, the heat flux through the lower part of the vehicle was 129 kW/m^2. Assuming the worst-case scenario in which the maximum heat flux is applied for 160 s as the pressure inside the gas storage tank drops to 1 bar, the calculated applied energy is 20.6 MJ/m^2, which is lower than the energy required to rupture the aforementioned hydrogen tank in the experiment.

Figure 12 shows the maximum temperatures generated in the three hydrogen storage containers of our model when the TPRD discharge angle was set at 45 and 90°. When jet flames were generated in Tank 1, the rearmost tank, the nearby temperature exceeded the operating temperature of the TPRD (110 °C) and activated the TPRDs of the other tanks. At a discharge angle of 45°, the temperatures of the nearby tanks decreased significantly after 5 s. Interestingly, the temperature of Tank 3, located farthest away from Tank 1, decreased below 80 °C. Therefore, setting the discharge angle of the TPRD to 45° or less reduces the probability of triggering TPRD operation in the nearby storage containers.

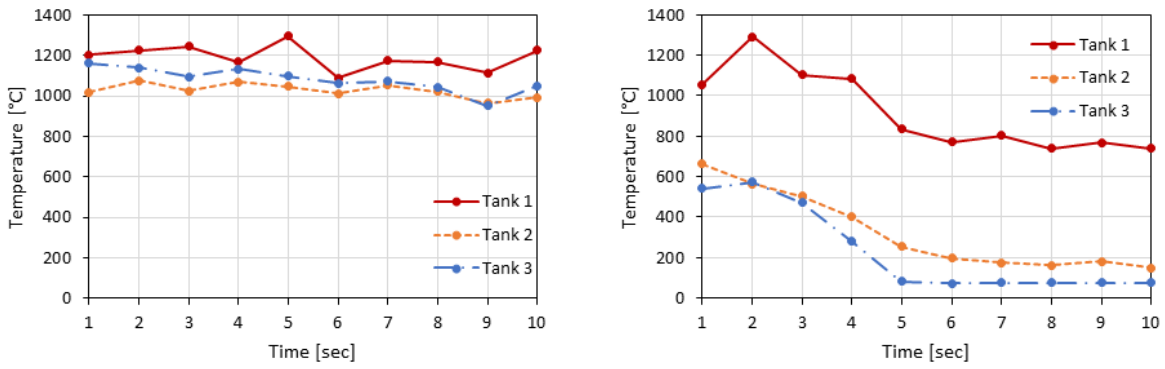

Figure 12. Maximum temperature of the hydrogen tanks at TPRD discharge angles of (**a**) 90° and (**b**) 45°.

3.4. Response Plan for Hydrogen Vehicle Accidents

In order to prevent the rupture of hydrogen storage containers, TPRD operation is automatically triggered at a certain temperature, like a sprinkler. However, the precise timing of this operation is unpredictable during a hydrogen car accident because it depends on the likelihood of the accident spread. Different response strategies, such as aggressive, marginal, and defensive strategies, should be employed at crash sites depending on the status of rescue targets and the possibility of flame propagation to the surrounding area. An aggressive response strategy aims to minimize damage from fires by actively eliminating risk factors through fire suppression. Marginal response strategies are mainly applied during the transition from an aggressive to a defensive strategy; when the rescue target is unlikely to survive or when a strong fire is spreading to surrounding flammables, it aims to remove any risk factors while accepting some damage. Finally, a defensive response strategy focuses on preventing fire expansion to minimize damage to the surroundings.

A systematic response to hydrogen vehicle accidents was devised and divided into three stages based on the status of the jet flames due to TPRD operation, as defined in

Table 2. Stage 1 begins at the point of the accident in which a fire breaks out, but jet flames are not present. At this stage, an aggressive response strategy should be adopted. First responders should wear protective equipment, especially over their lower bodies. Stage 2 begins at the onset of jet flames, where marginal or defensive strategies should be adopted depending on the status of the rescue targets. Additional protective measures should be taken during target rescue to protect all parties, followed by marginal rescue strategies. If no casualties are expected, a defensive strategy should be adopted to prevent damage to the surrounding area until the jet flames are extinguished. It is crucial to identify the number of hydrogen tanks in the accident vehicle and determine whether the TPRD of other tanks will be activated. In Stage 3, when the hydrogen in the hydrogen storage container has been expelled, and the risk of an explosion or jet flame has been eliminated, rescuers should respond as they would to a general vehicle accident. If jet flames do not occur due to TPRD malfunction, a defensive strategy should be employed, considering the risk of an explosion.

Table 2. Response strategies depending on the incident stage.

Stage	Definition	Strategies
1	The period immediately after a car accident, where a regular fire is present, resulting in flames and smoke, but no jet flames.	· Prioritize saving lives. · Wear protective gear to protect against sudden jet flames.
2	The period of jet flame generation, when it is difficult to access the vehicle without protective equipment.	· Determine if and how often jet flames occur. · Check the jet flame area with a thermal imaging camera. · Equip rescue target with protective gear. · If not urgent, wait until the jet flames subside.
3	The period after jet flames have subsided, in which the accident vehicle is still actively combusting.	· If there are no jet flames, assume a defensive strategy considering the risk of an explosion. · Apply general vehicle fire suppression methods. · Watch out for high-capacity battery thermal runaway. · Prevent the spread of fire to nearby areas.

Since the hydrogen tank of most hydrogen vehicles is located at the rear wheel axle, the heat flux distribution area shifts to the rear of the vehicle as the discharge angle of the TPRD decreases, as illustrated in Figure 9. The vehicle should ideally be approached in a diagonal direction from the front to minimize the effective area of the jet flame, as indicated by the arrows in Figure 13a. It is preferable to use the front doors rather than the rear doors for lifesaving activities inside the vehicle and to move the rescued person toward the front of the vehicle during evacuation.

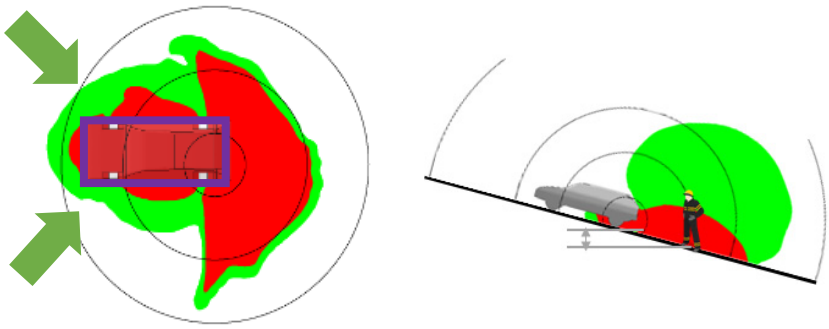

(**a**) (**b**)

Figure 13. Response considerations to hydrogen vehicle accidents. (**a**) Approach direction and (**b**) road gradient.

Hydrogen gas is light and diffuses easily into the air, and the tails of hydrogen jet flames rise as the pressure decreases. When responding to an incident involving a hydrogen vehicle parked on a slope, as depicted in Figure 13b, additional protective gear for the upper body is necessary, owing to the risk of damage occurring above the first responder's waist.

4. Conclusions

The use of eco-friendly cars has steadily increased in response to the global climate crisis. In South Korea, hydrogen vehicles have the least number of registrations among eco-friendly cars; however, their registrations are increasing at the highest rate. While accidents involving hydrogen vehicles have so far been rare, the risk of accidents will increase as more of these vehicles are used. Therefore, in this study, we devised an effective accident response plan for hydrogen vehicle accidents. The TPRD is a safety device used in hydrogen vehicles to prevent the hydrogen storage container from exploding by releasing hydrogen gas in the event of a fire. In doing so, a jet of flame is very likely to occur because of the wide flammability range of hydrogen. Numerical results show that the heat flux distributed around the vehicle moves from the center to the rear of the vehicle as the discharge angle of the TPRD decreases. This is advantageous for the safe evacuation of vehicle occupants, but the risk of secondary damage increases due to the heat flux generated beyond the rear of the vehicle. Our response plan utilizes a three-stage approach based on the status of the jet flames and employs aggressive, marginal, and defensive response strategies. We have determined that it is safest for first responders to approach hydrogen vehicles from the front in a diagonal direction. As the number and size of hydrogen tanks and their locations within vehicles may vary according to their manufacturer and model, first responders must identify safe access routes and specific hazards for each vehicle model. Manufacturers must also review the discharge angle of the TPRD in consideration of accident responses. In this study, we mainly analyzed the hazards caused by jet flames. Future studies must consider leaks and explosions to further develop accident response plans.

Author Contributions: Conceptualization, B.P. and O.K.L.; Methodology, Y.K.; Validation, J.O.P.; Formal Analysis, B.P.; Data Curation, O.K.L. and Y.K.; Writing—Original Draft Preparation, B.P. and O.K.L.; Writing—Review and Editing, O.K.L. and B.P; Visualization, B.P.; Supervision, Y.K.; Project Administration, B.P.; Funding Acquisition, B.P. All authors have read and agreed to the published version of the manuscript.

Funding: This research was funded by the Fire Safety Technology Research and Development Project for ESS and Hydrogen Facilities (Project No. 20019150) of the National Fire Agency.

Institutional Review Board Statement: Not applicable.

Informed Consent Statement: Not applicable.

Data Availability Statement: Not applicable.

Conflicts of Interest: The authors declare no conflict of interest.

References

1. EPA (United States Environmental Protection Agency). Sources of Greenhouse Gas Emissions. Available online: https://www.epa.gov/ghgemissions/sources-greenhouse-gas-emissions (accessed on 15 January 2023).
2. Samsun, R.C.; Rex, M.; Antoni, L.; Stolten, D. Deployment of Fuel Cell Vehicles and Hydrogen Refueling Station Infrastructure: A Global Overview and Perspectives. *Energies* **2022**, *15*, 4975. [CrossRef]
3. MOLIT (Ministry of Land, Infrastructure and Transport). Total Registered Motor Vehicles, MOLIT Statistics System. Available online: https://stat.molit.go.kr/portal/cate/statView.do?hRsId=58 (accessed on 30 May 2023).
4. Li, H.; Welsh, R.; Morris, A. Emergency Responders' Perceptions of Hydrogen Fuel Cell Vehicle: A Qualitative Study on the U.K. Fire and Rescue Services. *Int. J. Hydrog. Energy* **2021**, *46*, 32750–32761. [CrossRef]
5. Lim, O.K. Keyword Network Analysis of Domestic Research Articles for Determining Recent Trends of Hydrogen Refueling Stations. *Fire Sci. Eng.* **2021**, *35*, 83–90. [CrossRef]
6. Heino, O.; Kalalahti, J. Securing Operational Capability for Exceptional Circumstances: How Do Professional First Responders Respond to the Unexpected? *Sustainability* **2021**, *13*, 6418. [CrossRef]

7. Heino, O.; Takala, A.; Jukarainen, P.; Kalalahti, J.; Kekki, T.; Verho, P. Critical Infrastructures: The Operational Environment in Cases of Severe Disruption. *Sustainability* **2019**, *11*, 838. [CrossRef]
8. Hyundai. NEXO Emergency Response Guide. Available online: https://www.nfpa.org/Training-and-Events/By-topic/Alternative-Fuel-Vehicle-Safety-Training/Emergency-Response-Guides/Hyundai (accessed on 25 September 2022).
9. NFPA (National Fire Protection Association). Clarity Fuel Cell, 2017–18 Honda Clarity Fuel Cell Emergency Response Guide. Available online: https://www.nfpa.org/Training-and-Events/By-topic/Alternative-Fuel-Vehicle-Safety-Training/Emergency-Response-Guides/Honda (accessed on 25 January 2023).
10. Lee, K.; Kwon, M.; Kang, S.; Choi, J.; Kim, Y.; Lim, O.K. The Safety of Hydrogen Jet-Flame Suppression Training. *Fire Sci. Eng.* **2022**, *36*, 31–36. [CrossRef]
11. Park, B.; Kim, Y.; Lim, O.K. Training Program Analysis for Incidents in Hydrogen Refueling Stations. *J. Korean Soc. Hazard Mitig.* **2021**, *21*, 103–110. [CrossRef]
12. To, C.W.; Chow, W.K.; Cheng, F.M. Simulation of Possible Fire and Explosion Hazards of Clean Fuel Vehicles in Garages. *Sustainability* **2021**, *13*, 12537. [CrossRef]
13. Hussein, H.; Brennan, S.; Molkov, V. Hydrogen Jet Fire from a Thermally Activated Pressure Relief Device (TPRD) from Onboard Storage in a Naturally Ventilated Covered Car Park. *Hydrogen* **2021**, *2*, 343–361. [CrossRef]
14. FuelCellsWorks. Hyundai Nexo Takes Hyundai's Global Fuel Cell Vehicle Market Share to 51.7%. Available online: https://fuelcellsworks.com/news/hyundai-nexo-takes-hyundais-global-fuel-cell-vehicle-market-share-to-51-7 (accessed on 10 February 2023).
15. Birch, A.D.; Brown, D.R.; Dodson, M.G.; Swaffield, F. The Structure and Concentration Decay of High Pressure Jets of Natural Gas. *Combust. Sci. Technol.* **1984**, *36*, 249–261. [CrossRef]
16. Li, X.; Christopher, D.M.; Hecht, E.S.; Ekoto, I.W. Comparison of Two-Layer Model for Hydrogen and Helium Jets with Notional Nozzle Model Predictions and Experimental Data for Pressures up to 35 MPa. *Int. J. Hydrogen Energy* **2017**, *42*, 7457–7466. [CrossRef]
17. Houf, W.; Schefer, R. Analytical and Experimental Investigation of Small-Scale Unintended Releases of Hydrogen. *Int. J. Hydrogen Energy* **2008**, *33*, 1435–1444. [CrossRef]
18. Yu, X.; Yan, W.; Liu, Y.; Zhou, P.; Li, B.; Wang, C. The Flame Mitigation Effect of Vertical Barrier Wall in Hydrogen Refueling Stations. *Fuel* **2022**, *315*, 123265. [CrossRef]
19. Papanikolaou, E.; Baraldi, D.; Kuznetsov, M.; Venetsanos, A. Evaluation of Notional Nozzle Approaches for CFD Simulations of Free-shear Under-expanded Hydrogen Jets. *Int. J. Hydrogen Energy* **2012**, *37*, 18563–18574. [CrossRef]
20. Park, J.; Yoo, Y.; Kim, W. Analysis of Effect of Hydrogen Jet Fire on Tunnel Structure. *J. Korean Tunnelling Undergr. Space Assoc.* **2021**, *23*, 535–547. [CrossRef]
21. EIGA (European Industrial Gases Association). *Determination of Safety Distances*; IGC Doc. 75/07/E; EIGA: Brussels, Belgium, 2007; Volume 2007.
22. LaChance, J.; Tchouvelev, A.; Engebo, A. Development of Uniform Harm Criteria for Use in Quantitative Risk Analysis of the Hydrogen Infrastructure. *Int. J. Hydrogen Energy* **2011**, *36*, 2381–2388. [CrossRef]
23. NCD Risk Factor Collaboration (NCD RisC). A Century of Trends in Adult Human Height. *eLife* **2016**, *5*, e13410. [CrossRef] [PubMed]
24. Blanc-Vannet, P.; Jallais, S.; Fuster, B.; Fouillen, F.; Halm, D.; van Eekelen, T.; Welch, S.; Breuer, P.; Hawksworth, S. Fire Tests Carried Out in FCH JU Firecomp Project, Recommendations and Application to Safety of Gas Storage Systems. *Int. J. Hydrogen Energy* **2019**, *44*, 9100–9109. [CrossRef]